The influence of beam divergence on ion-beam induced surface patterns

R. Kree[a,*], T. Yasseri[a], A.K. Hartmann[b]

[a]*Institut. f. Theoretische Physik, Friedrich-Hund-Platz 1, Georg-August University Goettingen, D-37077 Goettingen, Germany*
[b]*Institut f. Physik, Universitaet Oldenburg, Carl-von-Ossietzky Str., 26111 Oldenburg, Germany*

Abstract

We present a continuum theory and a Monte Carlo model of self-organized surface pattern formation by ion beam sputtering including effects of beam profiles. Recently, it has turned out that such secondary ion beam parameters may have a strong influence on the types of emerging patterns. We first discuss several cases, for which beam profiles lead to random parameters in the theory of pattern formation. Subsequently we study the evolution of the averaged height profile in continuum theory and find that the typical Bradley-Harper scenario of dependence of ripple patterns on the angle of incidence can be changed qualitatively. Beam profiles are implemented in Monte Carlo simulations, where we find generic effects on pattern formation. Finally, we demonstrate that realistic beam profiles, taken from experiments, may lead to qualitative changes of surface patterns.

Key words: ion beam sputtering, pattern formation, beam divergence, continuum theory, Monte Carlo method
PACS: 68.55.-a, 68.35.Ct, 05.45.-a, 79.20.Rf, 81.16.Rf

1. Introduction

The control of pattern formation on solid surfaces during ion beam sputtering (IBS) has reached a considerable level of sophistication (see Ref.[1]). Under well defined processing conditions, it turns out that even changes in secondary ion-beam parameters like, for example, the beam profile may lead to different patterns [2, 3]. The current theoretical descriptions of pattern formation by IBS do not include secondary ion beam parameters and are therefore not able to explain any effects due to these parameters. Here, we make a first step towards a consistent continuum theory and a Monte Carlo model of the effects of ion beam profiles on pattern formation. We present some results of these descriptions, which confirm the non-trivial and important influence of beam profiles on the evolution of IBS induced patterns. In particular we show that both the proposed continuum theory and the Monte Carlo simulations imply substantial changes of the dependence of patterns on mean incidence angle, if non-trivial beam profiles are included.

2. Continuum Theory

Continuum theories of IBS, which are based upon the assumption of proportionality, $v_n \propto E(\mathbf{r})$, of the erosion velocity v_n and the power $E(\mathbf{r})$ deposited by the incident ions at a point $\mathbf{r}$ of the surface $\mathcal{S}$ have assumed that the ion beam is focused into a single direction of incidence. Here, we want to study cases, where v_n depends upon (random) ion beam parameters, and we will study beam profiles, described by a distribution of the angles of incidence of the beam, θ with repect to the z-axis and ϕ with respect the x-axis of the cartesian lab frame. The height $h(x, y, t)$, which describes the surface $\mathcal{S}$ in Monge representation, obeys the equation

$$\left\langle \frac{\partial h}{\partial t} \right\rangle = \left\langle \sqrt{g} \; v_n[\theta, \phi; h] \right\rangle \tag{1}$$

where $g = 1 + (\nabla h)^2$, and $\langle \cdots \rangle$ denotes an average over the beam parameters, which has to be specified further. Suppose that the beam is composed of ions incident at varying directions $\mathbf{m}$. Then we distinguish between three prototypical cases, defined as follows.

(i) *homogeneous subbeams*: Ion beams consisting of identical ensembles of subbeams of different directions $\mathbf{m}$ emanate from every point of the source illuminating the sample. The total power deposited at $\mathbf{r}$

is the sum of contributions from all subbeams and thus $\langle v_n \rangle = \int v_n(\mathbf{m}) p(\mathbf{m}) d^2 \mathbf{m}$, where $p(\mathbf{m})$ is the weight of subbeam $\mathbf{m}$ within the ensemble.

(ii) *temporally fluctuating homogeneous beam*: The substrate is illuminated homogeneously, but the direction constitutes a stationary, temporally homogeneous stochastic process $\mathbf{m}(t)$.

(iii) *spatio-temporally fluctuating beam*: The directions of incident ions form a homogeneous and stationary stochastic field $\mathbf{m}(x, y, t)$.

In all three cases, the average direction remains fixed, $\langle \mathbf{m} \rangle = \mathbf{m}_0$. For these cases we have performed the small slope and gradient expansion, which for an ideal beam starts with [4, 5],

$$\sqrt{g} v_n = -v_0(\theta) + w(\theta) \frac{\partial h}{\partial x} + a_x(\theta) \frac{\partial^2 h}{\partial x^2} + a_y(\theta) \frac{\partial^2 h}{\partial y^2} + \cdots .$$
(2)

To simplify the expressions, we will leave out noise in ϕ in the current work and concentrate on θ profiles for illustrative purposes. The full problem of ion beam noise will be discussed elsewhere. For cases (i) and (ii) Equ. (2) can be averaged term by term, but for case (iii) the expansions will produce additional terms containing spatial derivatives of θ. Here, we only consider smoothly varying direction fields, so that $|\nabla \theta| \ll |\nabla h|$. Then we find that such terms can be neglected.

We have studied the time evolution of $\tilde{h} = \langle h \rangle - \langle \int v_0 dt \rangle$ taking into account the linear terms depicted in Equ. (2). The linear evolution equation is written in the form $\partial_t \tilde{h} = \hat{L}(\theta) \tilde{h}$ with an operator $\hat{L} \tilde{h} := \hat{L}_{BH}(\theta) \tilde{h} - K \nabla^4 \tilde{h}$. $\hat{L}_{BH}$ includes the linear terms of v_n in Equ.(2), and $K \nabla^4 \tilde{h}$ is the simplest description of surface diffusion. We have considered two different beam profiles: (A) flat distributions of θ between $\theta_0 - \Delta\theta$ and $\theta_0 + \Delta\theta$ and (B) Gaussian distributions centred at θ_0. For homogeneous subbeam ensembles (case (i)), we can directly average the solution for every Fourier mode $\tilde{h}(k_x, k_y, t)$ over the single variable θ, $\langle \tilde{h}(\mathbf{k}, t) \rangle = \left\langle e^{\hat{L}(\mathbf{k}, \theta) t} \right\rangle h(\mathbf{k}, 0)$, whereas for the cases (ii) and (iii), further approximations are necessary to compute $\langle \tilde{h} \rangle$. If we restrict ourselves to the tractable case of small fluctuations $\delta\theta$ around θ_0, we may linearize $\hat{L}$ with respect to $\delta\theta$, i.e. $\hat{L}(\theta_0 + \delta\theta) \approx \hat{L}_0 + \delta\theta \hat{L}_1$, with $\hat{L}_1 = \partial \hat{L}_0 / \partial \theta$ depending upon primed quantities w', a'_x, a'_y, which are the derivatives of the coefficients in eq. (2) with respect to θ at θ_0. Then the beam fluctuations become multiplicative noise terms in the evolution equation for $\tilde{h}$ and can be treated by standard techniques (see Ref. [6] for a comprehensive overview). To illustrate the differences emerging from different models of the beam profile, we study the evolution of $\langle \tilde{h} \rangle$ for small Gaussian fluctuations in cases

(i), (ii) and (iii). For the latter two cases we assume that correlation times of θ are small, so that the white noise limit can be applied with respect to temporal fluctuations, i.e. $\langle \delta\theta(\mathbf{r}, t) \delta\theta(\mathbf{r}', t') \rangle = 2C(|\mathbf{r} - \mathbf{r}'|) \delta(t - t')$ (for case (ii), C is just a positive constant).

For *case (i)*, averaging $\exp(\delta\theta L_1(\mathbf{k})t)$ over Gaussian fluctuations leads to a drastic change of the growth law, $\langle \tilde{h}(\mathbf{k}, t) \rangle \propto \exp(\langle \delta\theta^2 \rangle L_1(\mathbf{k})^2 t^2 / 2)$, which quickly leaves the range of validity of the linear approximations involved. If, however, the Gaussian is replaced by the flat distribution (A), the growth law takes on the form $\propto t^{-1} \exp(rt)$ after a transient time. Even if the fluctuations are not considered small, the average can be performed by simple numerical integration and an effective rate can be extracted (not shown). For small fluctuations, this rate increases slightly above its value at $\Delta\theta = 0$, but for $\Delta\theta > 12.5°$ it decreases and falls well below the $\Delta\theta = 0$ value beyond $\Delta\theta \approx 20°$.

For cases(ii) and (iii) we can transform the averaged evolution equation $\partial_t \langle \tilde{h} \rangle = \hat{L}_0 \langle \tilde{h} \rangle + \langle \delta\theta \hat{L}_1 \tilde{h} \rangle$ into a closed equation for $\langle \tilde{h} \rangle$ making use of Novikov's theorem [6, 7]). For case (ii) it takes on the form $\partial_t \langle \tilde{h} \rangle = (\hat{L}_0 + C\hat{L}_1^2) \langle \tilde{h} \rangle$ and for case (iii) we obtain $\partial_t \langle \tilde{h} \rangle = [\hat{L}_0 + \hat{L}_1(\mathbf{r}')(C(\mathbf{r} - \mathbf{r}') \hat{L}(\mathbf{r}))|_{\mathbf{r}=\mathbf{r}'}] \langle \tilde{h} \rangle$. The terms arising from the Gaussian noise can be interpreted as renormalizations of the coefficients in $\hat{L}_0$, i.e. the averaged evolution equation becomes

$$\langle \partial_t h \rangle = \langle [\hat{L}_0 + \delta\theta \hat{L}_1] \tilde{h} \rangle = \hat{L}_0(w^R, a_x^R, a_y^R) \langle \tilde{h} \rangle \quad (3)$$

with the following renormalized coefficients: $w^R = w$ in both cases (ii) and (iii), $a_x^R = a_x + C w'^2$, $a_y^R = a_y$ for case (ii) and $a_x^R = a_x + a'_x(a_x + a_y)(\partial_x^2 C)_{\mathbf{r}=0}$, $a_y^r = a_y + a'_y(a_x + a_y)(\partial_y^2 C)_{\mathbf{r}=0}$ for case (iii). Explicit expressions for $w(\theta), a_{x/y}(\theta)$ can be taken from Ref. [5]. Note that for case (ii), there also appear third and (destabilizing) fourth order derivative terms, which will be discussed elsewhere. The renormalization due to homogeneous θ noise always contributes to a stabilization of the k_x modes, especially for larger θ_0. On the other hand, Fig. (3) illustrates, that for case (iii), beam profile noise can completely change the kinetic phase diagram of pattern formation. For simplicity, we have put $\sigma = \mu$. The typical Bradley-Harper scenario (upper panels: $\sigma = 2d$) with preferential growth of perpendicular ripples (crests parallel to the y-axis) at small incidence angles is depicted in the left upper panel. It is changed into a more complex scenario (right upper panel), which implies parallel ripples growing faster at small angles and an additional crossover region between $20^0 \cdots 30^0$ to perpendicular ripples due to a nontrivial beam profile. This scenario is very susceptible to other beam pa-

rameters, as depicted in the lower panels of Fig. (3), where we changed the extension of the collision cascade from $\sigma = 2d$ to $\sigma = d$. Here, the Bradley-Harper theory would only lead to faster growing parallel ripples whereas the beam divergence noise leads back to an extended region with dominant growth of perpendicular ripples.

3. Monte Carlo Simulations

Given the nontrivial nature of the averaging procedure inherent in the analytic continuum approach it seems also promising to study effects of beam profiles via Monte Carlo simulations. Within this method, realistic distribution functions of beam parameters and material specific diffusion models can be handled easily . Our simulation method has been described several times, more details can be found in Refs. [8, 9, 10, 11]. We use a lattice gas, solid-on-solid model. The discrete height profile $h(x, y, t)$ is updated via erosion steps and diffusion steps. An erosion step is initiated by choosing an ion, starting from a random position above the surface, then calculates the deposited energy at surface points (using Sigmund's formula[12, 4] $E(x', y', z') \propto \exp[-(x'^2 + y'^2)/(2\mu^2)] \exp[-(z' + d)^2/(2\sigma^2)]$ with an ion trajectory parallel to z' axis and the origin corresponds to the point of penetration) and sputters off a surface particle with a probability proportional to this energy. Diffusion steps consist of thermally activated hops of surface particles to unoccupied nearest neighbor sites. The kinetic barriers of this hopping consist of a constant term E_S due to the binding of the surface atom to the substrate, a bond-breaking term, which depends upon the numbers of in-plane neighbors of the initial and final site and an Ehrlich-Schwoebel barrier, which hinders the approach towards a downhill step of a terrace [13] and which may lead to anisotropic instabilities of a flat surface. In the following, we present results for case (iii), first using a flat distribution of incidence angles θ (B, see above) and then more realistic distributions from ref. [3]. Case (iii) is simulated by randomly choosing a position and an incidence angle for every ion. A most important parameter for pattern formation is the ratio of timescales τ_i/τ_d, where τ_i is the time between two incoming ions and τ_d is the time between two random hops. For typical fluxes of $\sim 10^{15}$ s^{-1} cm^{-2}, there is ~ 1 ion per atom per second, so $\tau_i \sim 1/L^2$ for a system with a flat $L \times L$ surface. For τ_d we take the waiting time for a hop over a substrate barrier $\tau_d = \tau_0 \exp(-E_S/(kT))$, which is ~ 0.01 s for 350K, $E_S = 0.75$ eV and a typical $\tau_0 \sim 10^{-13}$ s. In our simulations we have increased this typical ratio $\tau_i/\tau_d = 100/L^2$ by factors of $\sim 10^3$, which

enhances diffusion by slight changes in E_S or temperature.

First, let us discuss some generic results for situations, where patterns are formed mainly by erosion. In these runs, we exclusively used the flat distribution of incidence angles. Fig. 3 illustrates a generic slowing down of the pattern formation at average incidence angle $\theta_0 = 50°$ with increasing width of a flat distribution. But there are also some salient, qualitative effects of beam divergence on pattern formation, which can be observed. For $\theta_0 = 0$, i.e. sputtering at average normal incidence angle, we consider a parameter region, where neither ripples nor dots appear in case of an ideal, divergence-free beam. Fig. 3 depicts the structure function $S = \langle |h(\mathbf{k}, t)|^2 \rangle$ vs. k_x. Without beam divergence, there is no sign of a preferred wavelength. A beam divergence in θ leads to a maximum of S at a nonzero k_x, this maximum increases, if the beam is also widened in ϕ, thus a preferred wavelelngth of the surface patterns develops. To illustrate this effect, we show the limiting case of a flat distribution of ϕ over the entire interval $[0, 2\pi]$.

In Fig (3) a further generic effect of beam divergence is shown, which we expect to appear near the critical angle θ_c, which seperates the regimes of ripples perpendicular and parallel to the ion beam direction in $x - y$ plane. In this regime, the patterns depend very sensitively upon deteails of the beam properties and sudden qualitative changes of patterns under slight changes of incidence angle or beam profile may appear.

In a second series of simulations, we have tried to get closer to realistic conditions. We have used beam profiles, which resemble those of Ref. [3] and we have increased the ratio τ_i/τ_d by a factor of 1000, which would lead to surface structures emerging from Ehrlich-Schwoebel diffusion in the absence of erosion. In the right panel of Fig. (3) the ripple pattern is shown, which emerges after 3 monolayers of erosion without any beam divergence (beam direction parallel to the x-axis). With the beam profile corresponding to ref [3], the pattern shown in the right panel of Fig (3) results, which is composed of ripple patterns along $(1, 1, 0)$ directions. This same type of pattern is found for the ideal beam, if the ratio τ_i/τ_d is reduced by a factor of $\approx 10^3$. Thus it seems that a beam divergence enhances diffusion effects of Ehrlich-Schwoebel currents (which lead to islands with 45° edges). The presented example clearly illustrates that the type of pattern depends sensitively upon the beam profile and that there may be subtle interplays between effects from such secondary ion beam parameters and surface diffusion.

In conclusion, we have set up and studied a contin-

uum theory and a Monte Carlo model of IBS including ion beam profiles. In both approaches we have found clear indications of a rather strong dependence of surface patterns upon the special type of noise, which is produced by nontrivial ion beam profiles, as has been observed in experiments [1, 3, 2]. Whereas the continuum approach is most effective for small, Gaussian fluctuations, where it leads to a renormalization of coefficients of the local evolution equation of the average height profile, the Monte Carlo model is able to treat generic as well as more realistic and material specific situations. As the pattern forming scenarios depend sensitively on beam parameters and diffusion, such a modeling is neccessary, if one wishes to compare theoretical and experimental results in more detail. Our analysis also revealed that a comparison between continuum and MC results requires (i) the inclusion of non-linear effects in the continuum theory and (ii) simulations on longer time scales in MC modeling for small Gaussian fluctuations. These studies are currently under way.

References

[1] F. Frost, B. Ziberi, A. Schindler, and B. Rauschenbach. Surface engineering with ion beams: from self-organized nanostructures to ultra-smooth surfaces. *Appl. Phys. A*, 91:551–559, 2008.

[2] B. Ziberi, F. Frost, M. Tartz, H. Neumann, and B. Rauschenbach. Inportance of ion beam parameters on self-organized pattern formation on semiconductor surfaces by ion beam erosion. *Thin Solid Films*, 459:106–110, 2004.

[3] B. Ziberi, F. Frost, M. Tartz, H. Neumann, and B. Rauschenbach. Ripple rotation, pattern transitions and long range ordered dots on silicon by ion beam erosion. *Appl. Phys. Lett.*, 92:063102, 2008.

[4] R. M. Bradley and J. M. E. Harper. Theory of ripple topography induced by ion-bombardment. *J. Vac. Sci. Technol. A*, 6(4):2390–2395, Jul 1988.

[5] M. A. Makeev, R. Cuerno, and A. L. Barabási. Morphology of ion-sputtered surfaces. *Nucl. Instr. and Meth. in Phys. Res. B*, 197(3-4):185–227, Dec. 2002.

[6] J. Garcia-Ojalvo and J.M. Sancho. *"Noise in spatially extended systems"*. Springer, New York, 1985.

[7] E.A. Novikov. Functionals and the random force method in turbulence theory. *Sov. Phys. JETP*, 20:1290, 1965.

[8] A. K. Hartmann, R. Kree, U. Geyer, and M. Kölbel. Long-time effects in a simulation model of sputter erosion. *Phys. Rev. B*, 65(19):193403, May 2002.

[9] E. O. Yewande, A. K. Hartmann, and R. Kree. Propagation of ripples in monte carlo models of sputter-induced surface morphology. *Physical Review B (Condensed Matter and Materials Physics)*, 71(19):195405, 2005.

[10] E. O. Yewande, R. Kree, and A. K. Hartmann. Morphological regions and oblique-incidence dot formation in a model of surface sputtering. *Physical Review B (Condensed Matter and Materials Physics)*, 73(11):115434, 2006.

[11] E. O. Yewande, R. Kree, and A. K. Hartmann. Numerical analysis of quantum dots on off-normal incidence ion sputtered surfaces. *Physical Review B (Condensed Matter and Materials Physics)*, 75(15):155325, 2007.

[12] P. Sigmund. Theory of sputtering. i. sputtering yield of amorphous and polycrystalline targets. *Phys. Rev.*, 184(2):383–416, Aug 1969.

[13] M. Biehl. *Lattice gas models and Kinetic Monte Carlo simulations of epitaxial growth*. Birkhäuser, 2004.

Figure captions;

Fig.(1): Renormalization of both the parameter $a_x(\theta_0)$ and $a_y(\theta_0)$ from equ.(2) due to case (iii) beam profile noise are shown. The left upper and lower panel depict the behaviour for an ideal beam, (which already appeared in Ref. [4, 5]) (upper panel: $d/\sigma = d/\mu = 1$, lower panel:$d/\sigma = d/\mu = 2$, the right panels show the renormalization effects, if $\partial_x^2 C(0) = \partial_y^2 C(0) = 0.2$. *solid lines*: a_x, *dashed lines*: a_y. The lower curve corresponds to faster growth within linear theory. Note that the dependence of the dominant ripple orientation for ideal beams are changed completely due to the noise.

Fig.(2): Time evolution of the surfaces which are sputtered by an ion-beam with flat distribution profile. Horizontal axis is time (ion/lateral atom) and vertical axis is the value of width $\Delta\theta$ in degrees. θ_0=50°, $L = 256$ and ion energy is 1.0keV

Fig.(3): The modulus of structure factor of surfaces obtained from sputtering with non-zero ion beam divergence (limiting cases with $\Delta\phi = 0$ and $\Delta\phi = \pi$) compared to the case of sputtering by an ideal beam.

Fig.(4): Simulation results for $\theta_0 = 65°(\approx \theta_c)$, $\Delta\theta = 0°$ (left panel) and 20° (right panel) at t=2 ions/atom. Narrow bars indicate the azimuthal alignment of ion-beam.

Fig.(5): Simulation results of sputtering by an ion beam directed along the x-axis at an average angle of $\theta_0 = 50°$ for $t = 3$ ions/atom ($d/\sigma = 2, d/\mu = 4, d = 6$ lattice constants).*Left panel*: ideal beam, *Right panel*: Beam profile corresponding to [3]. Diffusion is determined by an Ehrlich-Schwoebel barrier of $E_{ES} = 0.15$ eV and an energy per bond of $E_b = 0.18$eV
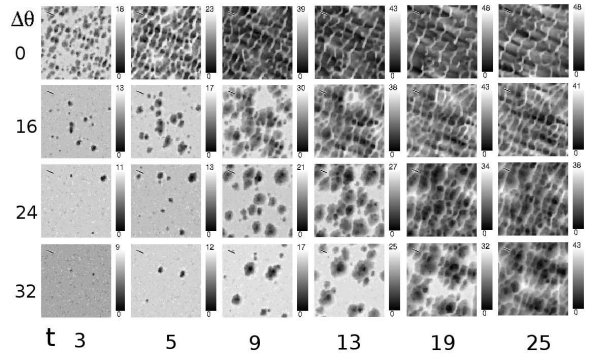

Figure 1: Renormalization of parameters ....

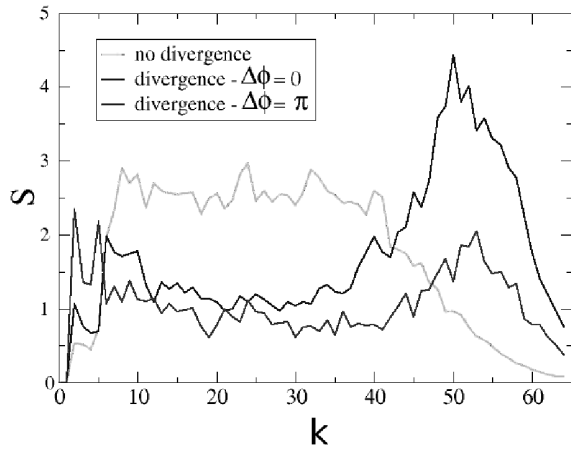

Figure 2: Time evolution of the surfaces ....

.

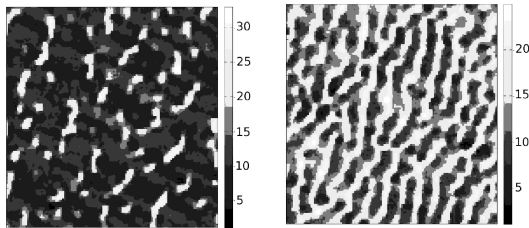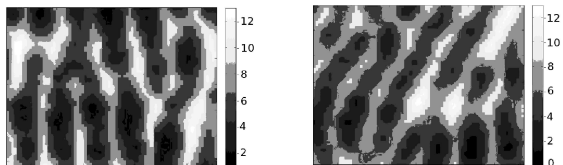Figure 3: The modulus of structure ....

Figure 4: Simulation results for ....

Figure 5: Simulation results of sputtering ....